Pre-mixed Partially Alloyed Iron Powder for Warm Compaction: KIP Clean Mix HW Series*


Yukiko Ozaki
Dr. Sci., Senior Researcher, Iron Powder & Magnetic Materials Lab., Technical Res. Labs.


Shigeru Unami
Senior Researcher, Iron Powder & Magnetic Materials Lab., Technical Res. Labs.


Satoshi Uenosono
Senior Researcher, Iron Powder & Magnetic Materials Lab., Technical Res. Labs.

Synopsis:

Kawasaki Steel has developed Japan's first iron powder pre-mix "Clean Mix HW Series" specially designed for warm compaction by incorporating "KW-wax", a lubricant with high performance during warm compaction process. KW-wax realized the powder characteristics—flow rate and apparent density—stable in the wide temperature range from room temperature to 423 K. Because of this stability, HW Series does not require the rigid control of the powder temperature in the compacting process of mass production. It was also found by the study about compacting process that KW-wax promoted particles rearrangement during compaction and gave green density higher than 7.3 Mg/m^3, having pore structures homogeneous in size and shape. The homogeneous structure of green compacts resulted in the improvement of mechanical strength of sintered and heat-treated compacts.

1 Introduction

The drive for downsizing various sintered component parts including automobile parts has been intense in recent years, and the development of high-strength iron powder and a high-density compaction process has long been awaited. Warm compaction process has been developed to manufacture cost-effective and highly-dense sintered products, of which density is equivalent to that attained by double pressing and double sintering (DPDS) process,[1,2] by compacting existing iron powder in a moderately-high temperature range of 393 to 433 K through one step process. Iron powder used for warm compaction is a type of segregation-free powder which is produced by making sub-material powder such as graphite powder adhere to iron powder using a binder, and then mixing with a lubricant. When used in warm compaction, the binder and lubricant to be added as well as iron powder itself affect the various powder characteristics. Kawasaki Steel has developed an innovative lubricant for warm compaction named "KW-wax" that has a high melting point and promotes the rearrangement of powder particles during compaction.[3] By incorporating KW-wax, the company commercialized Japan's first segregation-free pre-mixed iron powder for warm compaction under the trade name of "Clean Mix HW Series."

This paper introduces the Clean Mix HW Series iron powder pre-mix for warm compaction, which was developed based on the Ni-based partially alloyed iron powder "SIGMALOY 415S." This paper describes its powder characteristics in warm compaction, and the mechanical properties of warm-compacted and sintered compacts as well as warm-compacted sintered and heat-treated compacts. The paper focuses on the advantages of high-density compaction.

2 Experiments

2.1 Preparation of Test Specimens

2.1.1 Iron powder

Partially alloyed iron powder SIGMALOY 415S was used as the base iron powder. Its chemical composition was Fe containing 4 mass% Ni, 1.5 mass% Cu, and 0.5 mass% Mo. The compositions of iron powder premix used in the experiments are shown in **Table 1**. KW-wax is a mixture of a binder and lubricant developed for warm compaction. Material A was prepared using KW-wax. Comparative material B was prepared using zinc stearate, which is conventionally used as a lubricant for

* Originally published in *Kawasaki Steel Giho*, **33**(2001)4, 170–174

Table 1 Compositions of tested iron powders premixes

Material	Iron powder	Graphite (mass%)	Lubricant
A	KIP SIGMALOY 415S	0.3	0.6 mass% KW-wax
B	KIP SIGMALOY 415S	0.3	0.75 mass% Zinc Stearate
C	KIP SIGMALOY 415S	0	0.8 mass% KW-wax
D	KIP SIGMALOY 415S	0	Non-lubricant

Table 2 Pressing and sintering conditions in the preparation of specimens

Material	Pressing condition	Sintering condition
A	Warm compaction (403 K, 588 MPa)	N_2-10vol%H_2, 1 523 K, 3.6 ks
A	Warm compaction (403 K, 686 MPa)	
B	Cold compaction (298 K, 490 MPa)	
B	Cold compaction (298 K, 490 MPa)	
B	1st : Cold compaction (298 K, 686 MPa) 2nd: Cold compaction (298 K, 686 MPa)	1st : AX gas, 1 123 K, 1.8 ks 2nd: N_2-10vol%H_2, 1 523 K, 3.6 ks

powder metallurgy. Material C containing no graphite was prepared to investigate the powder behavior during warm compaction. Material D was solely composed of base iron powder and was prepared for comparison with material C.

2.1.2 Compacting and sintering conditions

Compacting and sintering conditions for materials A and B are as shown is **Table 2**. (For convenience sake, warm compaction and cold compaction are hereafter abbreviated as WC and CC respectively in the tables and figures.)

2.1.3 Heat-treatment conditions

Sintered materials obtained under the conditions listed in Table 2 were subjected to carburization for 9 ks at 1 193 K and carbon potential of 0.9 mass%, and then for 2.64 ks at 1 123 K and carbon potential of 0.7 mass%. They were next subjected to quenching in oil at 333 K and then to tempering for 3.6 ks in oil at 453 K.

2.2 Evaluation Method

2.2.1 Powder characteristics

Material A was heated to a specified temperature in a dry oven, and its flow rate and apparent density were measured in accordance with JIS Z 2502 and JIS Z 2504, respectively. Green compact was formed by a heater-equipped, tablet-type carbide die of inside diameter of 11.3 mm that was heated to a specified temperature. The density of the green compact was calculated from its weight and volume.

2.2.2 Compacting behavior in warm compaction

In order to confirm the effect of a lubricant in compacting behavior, material C that contained 0.8 mass% KW-wax and no graphite and comparative material D which was solely composed of base iron powder (SIGMALOY 415S) were subjected to warm compaction. The porosity, $\varepsilon(p)$ was measured as a function of compaction pressure, p during compaction. Compaction was carried out by the following procedure using a tablet-type die made of SKD steel with a diameter of 11.3 mm and a highly-precise universal testing machine. A lubricant was applied to the inside wall of the die, the temperature of which was controlled at 433 K. Test material weighted 7.5 g was filled into the die, then compressed up to the compaction pressure of 490 MPa at a constant cross-head speed of 1.67×10^{-4} m/s. At each level of compaction pressure (p), the amount of displacement of the punch $L(p)$ was measured. The volume reduction of the green compact $\Delta V(p)$ was calculated assuming that the cross-sectional area of the green compact being compressed does not cause spring-back and is equal to the cross-sectional area of the green compact when the compaction is completed. As for the compaction at 433 K, although the more precise values should strictly be calculated from the size of the green compact at exactly 433 K, due to difficulties of dimension measurement at the exactly equal temperature, the dimensions measured at ambient temperature were employed for the calculation. When the compaction was completed, the green compact was ejected from the die, weighed, and its diameter and height were measured by using a micrometer. The volume of the green compact when the compaction was completed was calculated from these values. The volume of the green compact at each level of compaction pressure was calculated by adding the value of $\Delta V(p)$ to the volume when the compaction was completed. The value of $\varepsilon(p)$ was calculate by Eq. (1) using $V(p)$ and the volume of material that has the true density of $V(\infty)$.

$$\varepsilon(p) = \{V(p) - V(\infty)\}/V(p) \cdots\cdots\cdots\cdots (1)$$

It was previously reported[4,5] that porosity $\varepsilon(p)$ and porosity reduction ratio $C_\varepsilon(p)$ during the compacting process in warm compaction are expressed by Eq. (2) after modifying the Cooper-Eaton model.[6,7]

$$\{\varepsilon(0) - \varepsilon(p)\}/\varepsilon(0) = a \exp(-b/p) + A \exp(-B/p) \cdots\cdots (2)$$

$$C_\varepsilon(p) = C_{\varepsilon,1}(p) + C_{\varepsilon,2}(p) \cdots\cdots\cdots\cdots\cdots (3)$$

where, a, b, A, B ($>b$) are constants, and the first and second terms of Eq. (2) correspond to the contributions

of particle rearrangement and those of plastic deformation, respectively. The value on the left-hand side of Eq. (3), $C_\varepsilon(p)$, was called the porosity reduction ratio. The constants in Eq. (2), a, b, A, and B were abtained from measured values by means of the non-linear least-squares method. The contributions of particle rearrangement and plastic deformation in the compacting process were estimated by comparing the magnitudes of the constants, a and A.

2.2.3 Green compact strength

Green compacts compacted into blocks of 10 mm in width × 35 mm in length × 3 mm in thickness were subjected to 3-point bending tests to evaluate their transvers rupture strength.

2.2.4 Mechanical strength of sintered compacts and heat-treated compacts, and pore distribution

Tensile strength, elongation, impact value, and Rockwell hardness were measured for each test specimen. In addition, contact fatigue strength was measured for warm-compacted, sintered and heat-treated compacts and DPDS-treated compacts. The contact fatigue strength measurement was carried out by the Mori-type, six-ball contact fatigue tester using disc specimens of 60 mm in diameter and 5 mm in height. Hertz stress was calculated by Eq. (4).[8)]

$$\sigma_W = 0.62(P/r^2)^{1/3}(1/E_1 + 1/E_2)^{-2/3} \quad \cdots\cdots\cdots (4)$$

where,

σ_W: Fatigue strength of the sintered material (MPa)
P : Load of the test ball (N)
r : Radius of the test ball (m)
E_1 : Young's modulus of the test ball (MPa)
E_2 : Young's modulus of the sintered material (MPa)

Further,

$$E_2 = -342\,000 + 69\,200\,\rho$$

where ρ is the density of the sintered material (Mg/m^3). The value of ρ was calculated using the volume of the specimen measured by Archimedes' method. Fatigue limits was determined by Hertz stress at 10^7 cycles duration.

The cut specimens were embedded in resin, and the cut surface was polished, but not etched. The polished surface thus prepared was photographed through an optical microscope, and the photographic image was loaded into a computer. The image was processed into two-level contrast, in which pores were shown by dark images. Using these images of pores, the number distribution of equivalent circle diameters of pores, and circularity factors of pores, were analyzed. The equivalent circle diameter of a pore was calculated as the diameter of a circle that has an area equivalent to the cross-sectional area of the pore. The circularity factor was calculated as (perimeter of a pore)^2 / (4π × cross-sectional area of the pore).

3 Results and Discussions

3.1 Temperature Dependence of Powder Characteristics

Figures 1 to **3** respectively show the temperature dependence of the flow rate and apparent density of material A, and the green density of material A compacted at a pressure of 686 MPa. Both the flow rate and

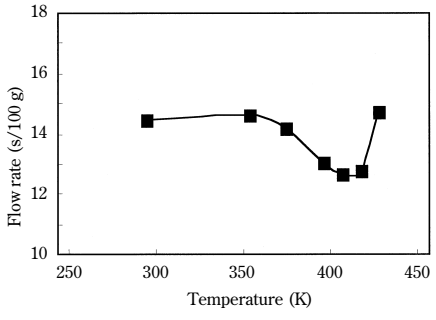

Fig. 1 Temperature dependence of flow rate for powder pre-mix of material A

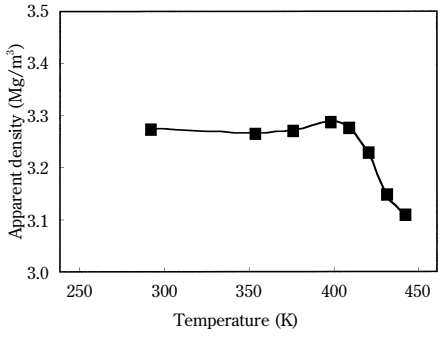

Fig. 2 Temperature dependence of apparent density for powder pre-mix of material A

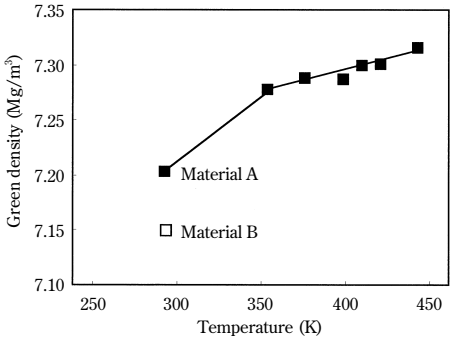

Fig. 3 Temperature dependence of green density for material A and green density of cold compacted material B

apparent density exhibit only small changes with temperature from ambient temperature to 423 K. This behavior apparently results from the fact that KW-wax has a high melting point and is less-sensitive to temperature changes, which provides the advantage that precise temperature control is not required during warm compaction of this material.

The green density of material A was higher than that of cold-compacted material B. The temperature dependence tended to decrease in a range beyond 373 K. Its high density at ambient temperature results from particle rearrangement promoted by KW-wax as will be described later. The decrease in the temperature dependence of the density in the high temperature range is considered as the result that KW-wax does not melt in this temperature region due to its high melting point and partially remains within the green compact.

3.2 Compacting Behavior in Warm Compaction

Figure 4 shows the compaction pressure dependence of the reduction rate of porosities of materials C and D at 433 K. The values observed in the experiment and those calculated by the regression equation are in a good agreement. Figure 4 also includes the values obtained for the first term, $C_{\varepsilon,1}(p)$, and the second term, $C_{\varepsilon,2}(p)$, in the regression equation. At a constant compaction pressure, material C exhibited a higher porosity reduction ratio than material D which was solely composed of iron powder, demonstrating the advantage provided by the lubricant KW-wax in obtaining a higher-density compact. Comparing $C_{\varepsilon,1}(p)$ and $C_{\varepsilon,2}(p)$ of each material, it is apparent that $C_{\varepsilon,1}(p)$ of material C increases steeply at a relatively low compaction pressure and then approaches a constant value. This behavior occurs because the lubricant KW-wax added to material C promotes the particle rearrangement even at a low compaction pressure and contributes to the densification of the powder. It was previously reported that the densification of material by

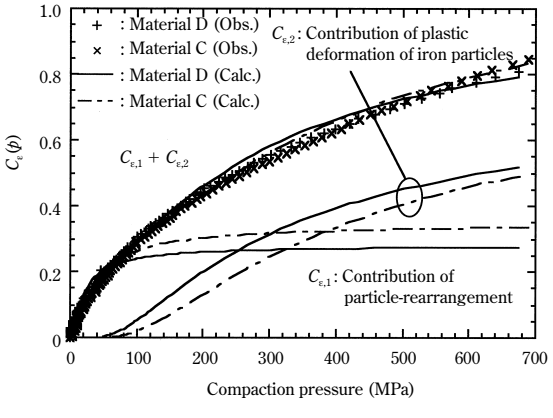

Fig. 4 Compaction pressure dependences of reduction rate of porosity, $C_\varepsilon(p)$, of powder premix C and powder D during warm compaction process

warm compaction is attributable to an increase of plastic deformation capability of iron powder by heating.[9] Thus, "HW Series" iron powder pre-mix with KW-wax can achieve high density in warm compaction due to not only the effects of increase in plastic deformation capability of an iron powder but also the promotion of particle rearrangement by KW-wax.

3.3 Green Compact Characteristics

Figure 5 shows the relation between compaction pressure and green density. Material A subjected to warm compaction achieved 7.31 Mg/m^3 at the compaction pressure of 686 MPa, exceeding the relative density of 95%.

Figure 6 shows the relation between green density and green strength of warm-compacted material A and that of cold-compacted material B. Compared with the extrapolated values for cold-compacted material B, warm-compacted material A exhibited a larger increase in strength than the increase in density. This behavior is explained as follows: in warm compaction, the plastic deformation capability of iron powder is enhanced by heating. As a result, iron powder particles easily undergo plastic deformation due to concentrating stress at contact points on their surfaces, and furthemore, strong bonding between iron powder particles are promoted because the additive is softened due to heating and is pushed into particle interstices.

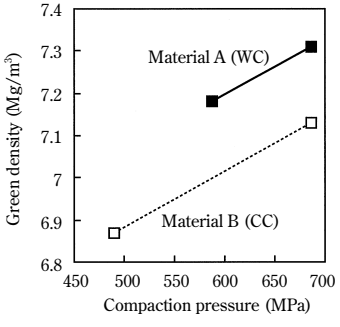

Fig. 5 Compaction pressure dependences of green density of materials A and B

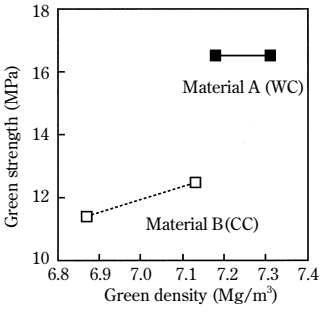

Fig. 6 Strength of green compacts for warm compacted material A and cold compacted material B

Table 3 Physical properties of as-sintered samples A and B sintered at 1 523 K for 3.6 ks in N_2-10vol%H_2

Material	Compacting condition	Sintered density (Mg/m^3)	Dimensional change (%)	Charpy impact value (J/cm^2)	Hardness (HRB)	Tensile strength (MPa)	Elongation (%)
A	Warm compaction, 588 MPa	7.35	−0.504	45	88	1 353	5.8
A	Warm compaction, 686 MPa	7.43	−0.405	56	90	1 445	6.9
B	Cold compaction, 490 MPa	7.06	−0.812	28	82	579	3.1
B	Cold compaction, 686 MPa	7.29	−0.625	41	85	619	4.7

Table 4 Physical properties of heat treated samples A and B

Material	Compacting condition	Density (Mg/m^3)	Charpy impact value (J/cm^2)	Hardness (HRC)	Tensile strength (MPa)	Elongation (%)	Contact fatigue strength (MPa)
A	Warm compaction, 588 MPa	7.35	35	44	1 424	1.1	2 691
A	Warm compaction, 686 MPa	7.43	38	45	1 316	0.4	2 913
B	Double press, double sinter	7.48	50	47	1 278	0.8	2 942

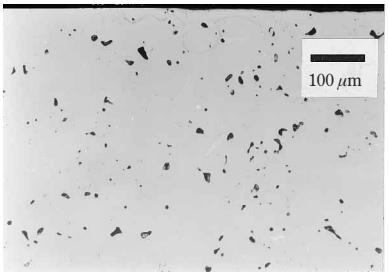

Photo 1 Microstructure near the surface of as-sintered material A

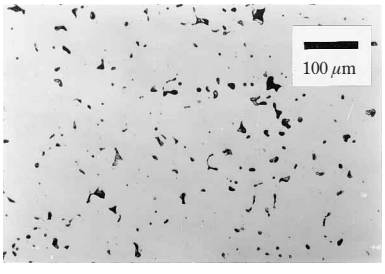

Photo 2 Microstructure of the center part of as-sintered material A

3.4 Mechanical Properties of Sintered Material and Heat-treated Material

Tables 3 and **4** show sintered density, dimensional change, Charpy impact value, hardness, tensile strength, elongation, and contact fatigue strength of sintered material and heat-treated material respectively.

The tensile strength, impact value and hardness increase in proportion to the increase in density, thus confirming the effect of densification by warm compaction. **Photos 1** and **2**, respectively, show the microstructures near the surface and in the center part of warm-compacted and sintered compact, having a density of 7.38 Mg/m^3. Pores are uniformly distributed both near the surface and in the center part. No difference in pore size is observable between the two photos. These photographs were subjected to image analysis.

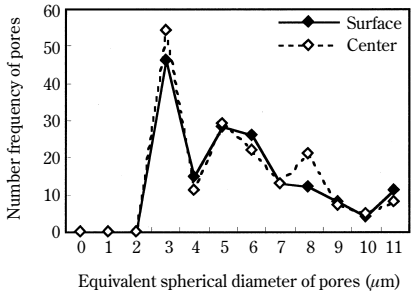

Fig. 7 Histograms of equivalent spherical diameters of pores in the center part and near the surface of as-sintered material A

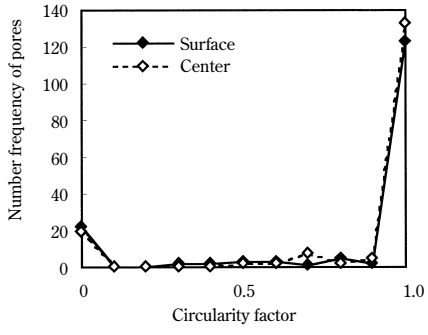

Fig. 8 Histograms of circularity factors of pores in the center part and near the surface of as-sintered material A

Figures 7 and **8** show histograms of equivalent circle diameter and circularity factor, respectively. The histograms of equivalent circle diameters of pores in the center part and near the surface were mostly overlapped as well as those of circularity factors of pores. Their median values are also similar each other, and both have a sharp distribution. The results indicate that nearly circular pores of size with narrow distribution are uniformly distributed near the surface as well as in the center part. It is suggested that densification was promoted by particle rearrangement during warm compaction. These findings are in good agreement with the

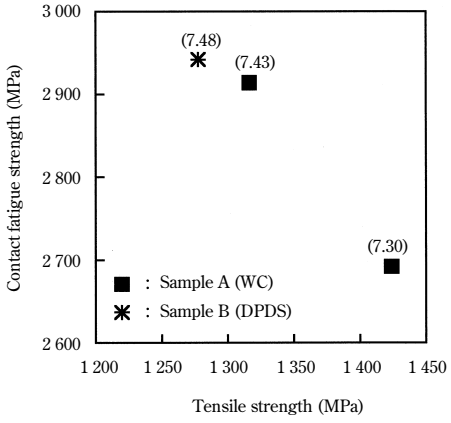

Fig. 9 Contact fatigue strength vs. tensile strength for heat treated specimens

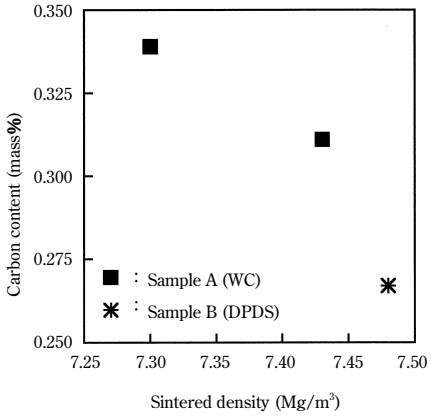

Fig. 10 Carbon content of heat treated specimens

results of analyzing the compacting behavior. The mechanical properties of warm-compacted and sintered material are thus improved not only by the increase in density but also by promotion of particle rearrangement, which leads to the uniform distribution of nearly circular pores of size with narrow distribution throughout the sintered compact.

From Table 4, it is found that the impact value and hardness increase with increasing density. **Figure 9** shows the relation between tensile strength and contact fatigue strength of heat-treated material. In this figure, numbers expressed in parentheses indicate densities. Contact fatigue strength increases with increasing density. In contrast, tensile strength decreases with increasing density. It was reported that the fatigue strength of sintered material is an index of the difficulty of crack generation in the surface area of a material, and fatigue strength increases with an increase in circularity of pore on the surface, a decrease in number of pores, and a decrease in diameter of pores in the surface area.[9] The increased contact fatigue strength demonstrated in Fig. 9 is thus considered to be attributable not only to increased density (i.e., decreased porosity) but also to the circularity and size uniformity of pores in the surface as shown in Figs. 7 and 8. Tensile strength is affected by density, and also depends on surface condition as it is related to susceptibility to crack generation, and therefore is affected by the amount and depth of carburization.

Figure 10 shows the relation between density of heat-treated material and its carbon content increased by carburization. When the density is increased beyond around 7.3 Mg/m^3, the amount of carburization decreases. This behavior is interpreted that a decrease of the porosity in the surface area with an increase of density, in particular a decrease the ratio of open pores suppresses carburization.

Further improvement in tensile strength is expected when the carburizing conditions is optimized with regard to warm-compacted, sintered and heat-treated material as well as DPDS-treated material, of which task is set as a future task.

4 Conclusions

(1) KW-wax suitable for warm compaction has been developed for use in warm compaction, and iron powder pre-mix for warm compaction "Clean Mix HW Series" has been commercialized. The product exhibits powder characteristics as listed below when used in warm compaction. Since these characteristics are not easily affected by the powder temperature variation, which is encountered in mass-production processes, the developed products provide the ease of temperature control.
   (a) The flow rate and apparent density remain stable in a range of ambient temperature to 423 K, irrespective of temperature variations.
   (b) Green density is more than 7.30 Mg/m^3 when compacted at a pressure of 686 MPa. The temperature dependence of green density is small in a range beyond 373 K.
   (c) It was found that high density in warm compaction is achieved by the increase in plastic deformation capability of iron powder and furthermore by particle rearrangement which is promoted by adding the KW-wax.

(2) Analysis of the compacting behavior of HW Series iron powder pre-mix ascertains that KW-wax plays a role to promote particle rearrangement. It was made ascertained that particle rearrangement helps achieve higher densities for material prepared by warm-compacting, sintering, and that prepared by warm-compacting, sintering and carburizing heat-treatment process, and further helps provide a microstructure in which nearly circular pores of sizes with sharp distribution are uniformly distributed, thereby improving the mechanical properties.

(3) The tensile strength of materials which are prepared

by a process of warm-compacting, sintering and carburizing heat-treatment, tends to decrease with increasing density. This behavior is interpreted that the decrease in ratio of open pores in the surface area with increase in density, suppresses carburization inside materials. In the gas-carburizing treatment of warm-compacted and sintered material, a future issue is to optimize the carburizing conditions.

References

1) S. H. Luk, H. G. Rutz, and M. Lutz: "A New Method for Manufacturing High Performance Powder Metallurgy Components", Advances in Powder Metallurgy and Particulate Materials, MPIF, Princeton (USA), 5(1994), 135
2) H. G. Rutz and F. G. Hanejko: "High Density Processing of High Performance Ferrous Materials", Advances in Powder Metallurgy and Particulate Materials, MPIF, Princeton (USA), 5(1994), 117
3) Y. Ozaki, S. Uenosono, and S. Takajo: "Compaction Phenomena in Heated Dies and Characteristics of Sintered Body of Segregation-free Iron Powder with Heatproof Lubricant." Proc. of Spring Conf. of Jpn. Powder and Powder Metallurgy 1A-11, (1999), 92
4) Y. Ozaki, S. Uenosono, and K. Ogura: "Compaction Phenomena of Iron Powder in Dies—An Analysis of Compaction Phenomena in Warm Compaction.", *CAMP-ISIJ*, **10**(1997), 1066
5) Y. Ozaki, S. Uenosono, and K. Ogura: "An Analysis of the Compaction Behaviors of Iron Powder", Advances in Powder Metallurgy and Particulate Materials, MPIF, Vancouver (CAN), 2(1999), 109
6) A. R. Cooper and L. E. Eaton: *J. Amer. Ceram. Soc.*, **45**(1962), 97
7) H. Hashimoto, R. Watanabe, and H. Isako, "Compaction Equations for Atomized Low Alloy Steel Powders", Recent Prog. in Iron Powder Metallurgy, The Iron and Steel Inst. of Jpn., Tokyo, (1996), 39
8) K. Ogura, S. Takajo, Y. Maeda, J. Kotsuki, and K. Sakurada: *Kawasaki Steel Giho*, **21**(1989)3, 250
9) P. Beiss and M. Dalic: "Effect of Pore Structure on Bending Fatigue Strength of Sintered Steel", Advances in Powder Metallurgy and Particulate Materials, MPIF, Washington (USA), 13(1996), 249